REPORT DOCUMENTATION PAGE

Public reporting burden for this collection of information is estimated to average 1 hour per response, including the time for reviewing instructions, searching existing data sources, gathering and maintaining the data needed, and completing and reviewing the collection of information. Send comment regarding this burden estimates or any other aspect of this collection of information, including suggestions for reducing this burden, to Washington Headquarters Services, Directorate for information Operations and Reports, 1215 Jefferson Davis Highway, Suite 1204, Arlington, VA 22202-4302, and to the Office of Management and Budget, Paperwork Reduction Project (0704-0188), Washington, DC 20503.

1. AGENCY USE ONLY *(Leave blank)*	2. REPORT DATE	3. REPORT TYPE AND DATES COVERED Technial Report

4. TITLE AND SUBTITLE

TITLE ON TECHNICAL REPORT

5. FUNDING NUMBERS

DAAG55-98-1-0277

6. AUTHOR(S)

AUTHOR(S) ON TECHNICAL REPORT

7. PERFORMING ORGANIZATION NAMES(S) AND ADDRESS(ES)

Boise State University

8. PERFORMING ORGANIZATION REPORT NUMBER

9. SPONSORING / MONITORING AGENCY NAME(S) AND ADDRESS(ES)

U.S. Army Research Office
P.O. Box 12211
Research Triangle Park, NC 27709-2211

10. SPONSORING / MONITORING AGENCY REPORT NUMBER

ARO 37739.5-EV-DPS

11. SUPPLEMENTARY NOTES

The views, opinions and/or findings contained in this report are those of the author(s) and should not be construed as an official Department of the Army position, policy or decision, unless so designated by other documentation.

12a. DISTRIBUTION / AVAILABILITY STATEMENT

Approved for public release; distribution unlimited.

12 b. DISTRIBUTION CODE

13. ABSTRACT *(Maximum 200 words)*

ABSTRACT ON REPRINT

20011113 165

14. SUBJECT TERMS	15. NUMBER IF PAGES
	16. PRICE CODE

17. SECURITY CLASSIFICATION OR REPORT	18. SECURITY CLASSIFICATION OF THIS PAGE	19. SECURITY CLASSIFICATION OF ABSTRACT	20. LIMITATION OF ABSTRACT
UNCLASSIFIED	UNCLASSIFIED	UNCLASSIFIED	UL

HYDROGEOLOGICAL PROPERTY ESTIMATION USING TOMOGRAPHIC DATA AT THE BOISE HYDROGEOPHYSICAL RESEARCH SITE

John E. Peterson, Jr., Ernest L. Majer;
Lawrence Berkeley National Laboratory, Earth Sciences Division, Berkeley, CA 94720
Michael D. Knoll; *CGISS, Boise State University, Boise, ID 83725*

ABSTRACT

Crosswell seismic and radar data were acquired at the Boise Hydrogeophysical Research Site (BHRS) as part of an effort to characterize the hydrological property distribution in a heterogeneous alluvial aquifer. The dielectric constant and amplitude attenuation values obtained from inversion of the radar data, as well as the seismic P-wave velocity values obtained from inversion of the seismic data, reveal similar spatial patterns. Comparison of this tomographic information with coincident wellbore logs suggest that the geophysical attributes are sensitive to hydrogeological variations. Information obtained from the radar tomography data were used to produce 2-D, high-resolution images of porosity and electrical conductivity. Comparison of these images with coincident log data reveal that these estimates are reasonable and suggests that the tomography data will be useful at this site for delineating variations in hydrological parameters.

INTRODUCTION

The Boise Hydrogeophysical Research Site (BHRS) is being developed in Boise, Idaho for hydrologic and geophysical research in a shallow alluvial aquifer comprised of unconsolidated sands and cobbles. At the time of this survey the water table was about 2.5 meters below land surface at tested wells; interpretation of geophysical data in this study is limited to the saturated section. A goal of the research is to use this site to develop and test hydrologic and geophysical methods for characterizing the distribution of hydrogeological properties in heterogeneous alluvial aquifers (Barrash and Knoll, in Press, Barrash and others, 1999). As part of this research, Lawrence Berkeley National Laboratory (LBNL) acquired high-resolution crosswell tomographic seismic and radar data in October, 1997. The crosswell data were collected to characterize the acoustic and electromagnetic velocity and attenuation structure of the site and to study differences in the information that these two geophysical methods offer. Correlation of these seismic and radar attributes with borehole log data permits elucidation of the relationships between geophysical and hydrological parameters at this site. Some of the radar data were acquired at a lower frequency to study the effects of frequency content on the resolution of structural features. The geophysical data can be used with developed petrophysical relationships to provide high-resolution, multi-dimensional estimates of hydrologic parameters; the development of these site-specific relationships is in progress. Here, we present examples of the use of tomographic radar and seismic data with petrophysical relationships borrowed from literature to illustrate how we will use these data to both delineate structural features and to map porosity variations.

For the moderate- to coarse-textured materials at this site, and for the high excitation frequencies utilized, the radar velocity, v, in the medium is dependent on the dielectric constant of the material through the equation:

$$v = \frac{c}{\sqrt{\kappa}} \qquad (1)$$

where c is the velocity of electromagnetic waves through air and κ is the bulk dielectric constant. As the dielectric constant of air is 1, of water is 80, and of sand grains about 3-5, saturated and higher porosity material will have a higher dielectric constant than the corresponding unsaturated or lower porosity material due to the presence of water in the pore space. The velocity fields for each of the three well pairs obtained from the inversion procedure were converted to dielectric constant using (1).

The measured bulk dielectric constant can be expressed as a function of the components of a system using a mixing model. For a two-phase saturated system composed of matrix material and water-filled pore space, this model is given by:

$$\kappa \approx [(1-\varphi)\sqrt{\kappa}_m + \varphi\sqrt{\kappa}_w]^2 \qquad (2)$$

where φ is porosity, subscripts m and w refer to matrix and water components, respectively. We assume here that the dielectric constant of the matrix sand and cobble material at the BHRS is fairly constant. With this assumption, equation (2) suggests that any changes in bulk dielectric constant are a function of variations in porosity. For a matrix dielectric constant of approximately 4 and a water dielectric constant of 80, equation (2) reduces to:

$$\kappa \approx 4 + 27.78\,\varphi + 48.22\,\varphi^2 \qquad (3)$$

200 MHz

100 MHz

Figure 2. The frequency response of the received 200 MHz and 100 MHz radar signals.

Three radar tomographic profiles, B1-B2, B1-C1, and B2-C1 were collected between three wells which form a triangle with sides of 3.41, 5.21 and 4.70 meters, respectively (Figure 1). The radar tomography data were acquired using the Sensors and Software pulseEKKO 100 ground penetrating radar system. Radar profiles were collected with 200 MHz antennas and profile B1-C1 was additionally acquired using 100 MHz antennas to study resolution variations as a function of acquisition frequency. The radar data were collected with 0.25 meter source and receiver spacing between the depths of 1 to 18 meters below ground surface to obtain radar tomographic coverage over angles of approximately 0 to 70 degrees. In addition to acquiring the full tomographic data, Zero Offset Profiles (ZOP) were run before and after each survey to determine the drift in zero time which is necessary for data processing as described in Peterson and Williams (1997).

Figure 1. Plan view of the tomography wells at the BHRS.

Good signal quality was obtained for all offsets of each well pair. A typical frequency content of the signals received for the 200 MHz antennas is shown in Figure 2a which illustrates that the peak energy is at about 80 MHz. The 100 MHz signal produces peak energy at about 40 MHz (Figure 2b). These central frequencies are independent of the three borehole separation distances. The data quality at these distances and angular offsets suggests that radar data may be acquired at 12 to 15 meter well separations using 200 MHz antennas and at 15 to 20 meters using 100 MHz antennas at the BHRS.

The first arrival times of the electromagnetic energy were picked for each survey, producing about 3000 to 4000 travel times for each data set. An Algebraic Reconstruction Technique, or ART (Peterson et al., 1985), was used to invert the electromagnetic wave travel time data to obtain the velocity distribution. This program assumes that the energy travels as straight ray paths between source and receiver, and also takes into account radar source and receiver statics which were determined for each source and receiver location. The static corrections result in travel time shifts which compensate for variations in the borehole, very small-scale structures immediately adjacent to the borehole, and antenna-borehole coupling effects. The ART algorithm produced a grid composed of 0.20 meter square pixels of constant velocity, or a two-dimensional velocity image of the intra-borehole area in the saturated section.

631
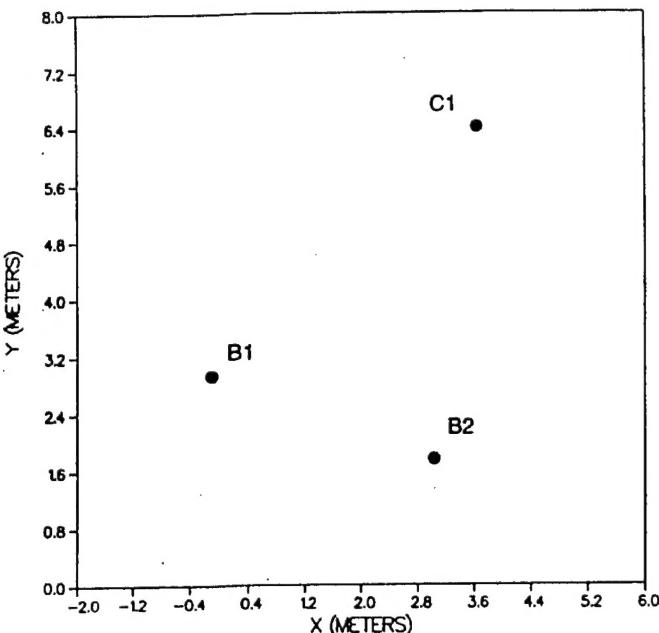
Using (3), the dielectric constant values obtained from the velocity data were converted into porosity images (Figure 3). Each image displays a similar porosity structure with two well-defined zones of high porosity at approximate depths of 6 and 12.4 meters. A deeper high porosity zone at 15 meters is not as well-defined as the upper two zones. Another high porosity feature is observed on the B1-C1 and B2-C1 tomograms at a depth of about 5 meters.

Neutron logs, available from all three wells, were used to calculate porosity. Adjusted porosity values from the neutron log information are plotted to the left and right of the tomograms displayed in Figure 3. Although the logs from each borehole are significantly different from each other, they correlate well with the co-located porosity estimates obtained from the tomography data. For example, high porosity regions coincide at depths of 6, 12 and 15 meters in well B2 (the B1-B2 and B2-C1 tomograms). The high porosity feature at a depth of 6 meters in the B2 porosity log appears at a depth of 5 meters on the borehole C1 porosity log. The B2-C1 porosity tomogram (Figure 3), however, indicates that this is not a continuous dipping feature as would be interpreted using log correlation, but two distinctive layers, neither of which extend the length of the tomogram. A high porosity zone at the 15 meter depth is thicker, but less porous on the C1 porosity log than on the B2 log; this is also observed on tomogram B2-C1. The porosity log from borehole B1 shows numerous fluctuations, with less well-defined high- and low-porosity zones than the B2 and C2 logs. The B1-B2 and the B1-C1 tomograms, however, indicate distinct zones of high and low porosity above depths of 13 meters and do not display the fluctuating porosity observed on the B1 porosity log.

Radar attenuation information can also be obtained from the crosshole radar data. The amplitudes are measured by taking the root mean squared value of approximately half cycle of the first arrival. The attenuation is calculated by inverting the waveform amplitudes using the same algorithm, geometry, and input values as were used to obtain the velocity tomograms. In low-attenuating media (from 0.02 to 10 dB/m) and at the high excitation frequencies used for this experiment, the attenuation is related to the conductivity of the material through the equation (Davis and Annan, 1989):

$$\sigma[S/m] \approx \alpha[dB/m]\frac{\sqrt{\kappa}}{1640} \tag{4}$$

The attenuation tomograms were converted to electrical conductivity tomograms using this relation and are shown in Figure 4. These conductivity tomograms are coincident with the attenuation tomograms; the dielectric constant had little effect on the conductivity because the relative range in dielectric constant values was small relative to the range in attenuation values. Also shown, to the left and right of the crosswell images, are the measured electrical conductivities obtained from borehole induction logs which have been arithmetically averaged over 20 cm depth intervals so that the log and radar tomogram sampling intervals are equivalent. The conductivity images show anomalies in the same regions as the porosity distributions (Figure 3). For example, a low conductivity zone is coincident with the high porosity zone at a depth of 6 meters, and on either side of this layer are high conductivity zones which are especially strong in the B1-C1 and B2-C1 tomograms. A low conductivity zone, observed in all the tomograms at a depth of 12 meters, is also coincident with the high

632

porosity zone at that depth. There is a high conductivity zones immediately below this high conductivity layer. There is no coinciding conductivity anomaly near the high porosity zone observed in all tomograms at a depth of 15 meters, and the area between the two low conductivity layers appears more heterogeneous than was observed in the porosity tomograms.

A crosswell survey was also performed from B1-C1 at a frequency of 100 MHz instead of 200 MHz to study the effects of excitation frequency on spatial resolution and hydraulic parameter estimation. The station spacing and inversion parameters were the same as for the 200 MHz surveys. The resulting porosity image obtained from the dielectric constants and equation (3) is shown in Figure 5. The same three zones of high porosity are still observed in this image, but the zones are less distinct and the absolute porosity values are not as high. More importantly, the smaller high-porosity zone at a depth of 5 meters, which was observed on the 200 MHz profile, is not as easily observed and cannot be spatially distinguished from the 6 meter zone. Also, the high-frequency tomogram resolved some structure in the region between 6 to 12 meters, whereas the low frequency tomogram did not. The lower resolution obtained with the 100 MHz data are due to the increased wavelengths; the wavelengths of this data are twice as long as the wavelength of the 200 MHz data, so larger amounts of material are sampled and effectively averaged with the 100 MHz data than with the 200 MHz data.

ACQUISITION AND ANALYSIS OF SEISMIC TOMOGRAPHY DATA

Seismic P-wave tomographic data were also acquired between the same boreholes as the radar data (Figure 1). The data for the well pair with shorter separation (B2-B1) was of much better quality than the other well pairs. While there was a marked decrease in amplitudes for the data with the farther borehole separation (B2-C1), the poor quality of this data was primarily due to a problem in the acquisition equipment. The peak frequency of the seismic data was 4000 Hz. Based on this data and prior experience with this system, good quality data should be achievable at the BHRS for well separations up to 8 to 10 meters.

The seismic data were inverted in the same manner as the radar data; the resulting seismic velocity image for B1-B2 is shown in Figure 6. The velocity structure appears to offer similar resolution as the porosity estimates obtained from the radar data in the B1-B2 well pair (Figure 3). Comparison of these data suggests that seismic velocity increases as porosity increases. Seismic attenuation tomograms could not be produced at this time due to errors in recording the gain applied at acquisition. Observations of the data show that the signals are almost entirely attenuated in the low velocity feature at 6 meters, but not at the 12 meter low velocity zone.

CONCLUSIONS

High-resolution images of dielectric constant, electromagnetic wave attenuation, and seismic velocity were obtained using radar and seismic borehole tomography methods. Radar frequencies of 200 MHz and seismic frequencies of 4000 Hz appear to provide similar resolution of features, with a wavelength of approximately 0.6 meters. Lower frequency seismic data will produce farther acquisition offsets, but as shown in the radar data, there can be a significant loss of information with any drop in frequency. Preliminary analysis of borehole neutron and induction logs and seismic and radar tomography data suggests that:

1) The higher resolution offered by the 200 MHz radar data delineate the interwell variability more clearly than the coincident 100 MHz data,

2) There is a direct correspondence between porosity and dielectric constant obtained from radar tomography travel time data,

3) The estimated porosities, obtained from the dielectric constant estimates and petrophysical mixing model compare favorably with the porosities obtained from the neutron probe,

4) Electrical conductivity from borehole induction logs correspond with conductivity estimated using radar tomography travel time and amplitude information,

5) There is an inverse relationship between electrical conductivity and porosity,

6) There is a direct correspondence between the seismic P-wave velocity tomograms and the porosity tomograms estimated from the radar velocity values.

The information produced by the well and tomography data, as well as laboratory core data, will enable development of site-specific relationships between geophysical and hydrogeological parameters. These relationships will then be used with the tomography data to provide multi-dimensional profiles of hydrogeological parameters with a 0.20 meter resolution.

ACKNOWLEDGEMENTS

REFERENCES

Barrash, W., and M.D. Knoll, in press, Design of research wellfield for calibrating geophysical measurements against hydrologic parameters: 1998 Conference on Hazardous Waste Research, Snowbird, UT, Great Plains/Rocky Mountain Hazardous Substance Research Center, Kansas State University.

Barrash, W., T. Clemo, and M.D. Knoll, 1999, Boise Hydrogeophysical Research Site (BHRS): Objectives, design, initial geostatistical results: SAGEEP'99, Oakland, CA.

Davis, J.L. and A.P. Annan, Ground-penetrating radar for high-resolution mapping of soil and rock stratigraphy, *Geophysical Prospecting*, 37, 531-551, 1989.

Peterson, J.E., Jr. and K.H. Williams, Ground Penetrating Radar Results at the Box Canyon Site: 1996 Survey as part of Infiltration Test, *LBNL-Report-40915*, 1997.

Peterson, J.E., B.N.P. Paulsson and T.V. McEvilly, Applications of algebraic reconstruction techniques to crosshole seismic data, *Geophysics,* 50, 1566-1580, 1985.
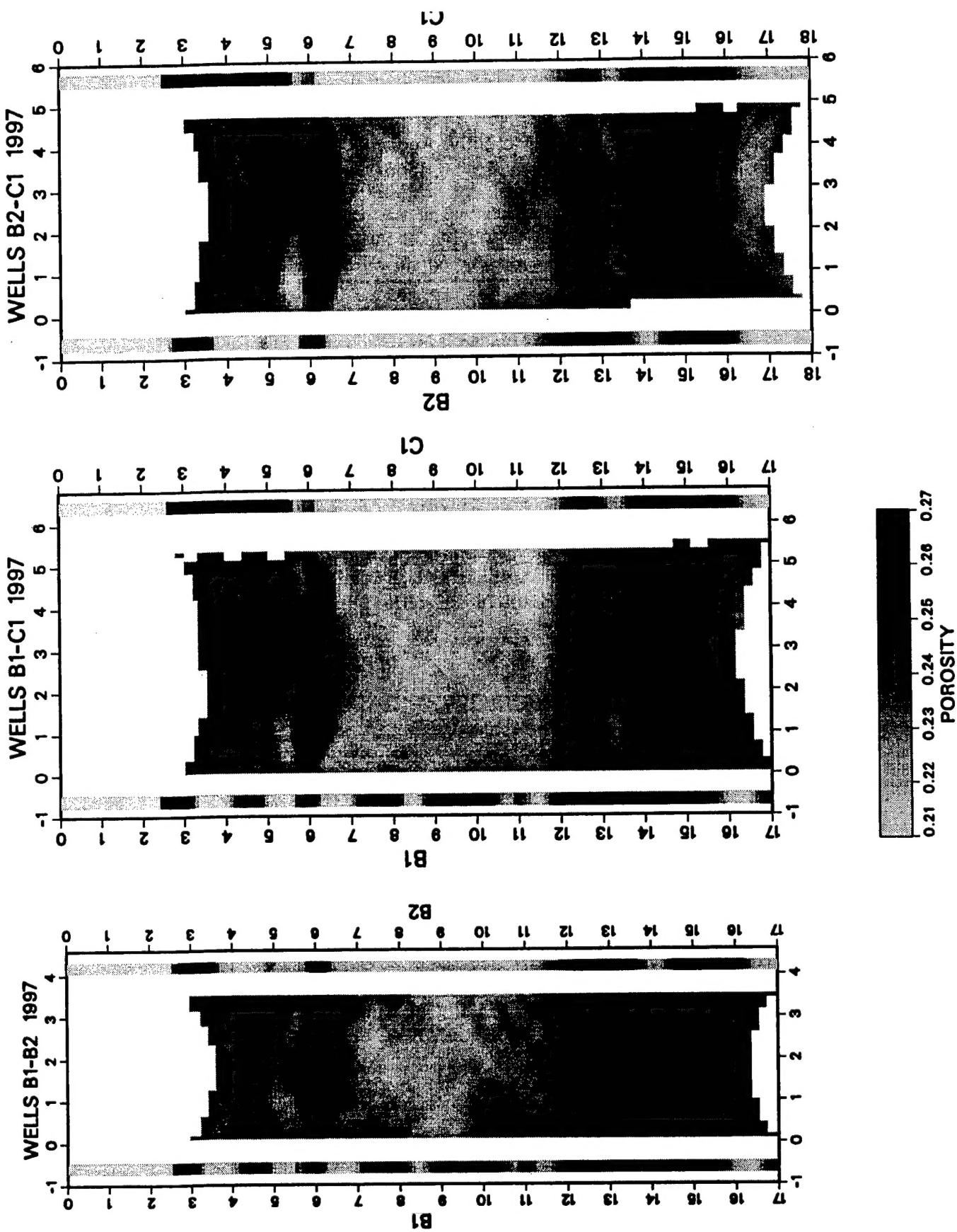
Figure 3. Porosity tomograms, calculated from the dielectric constants values using Equation (3). Adjusted porosity logs are plotted in grey-scale format on either side of the radar tomograms.

636
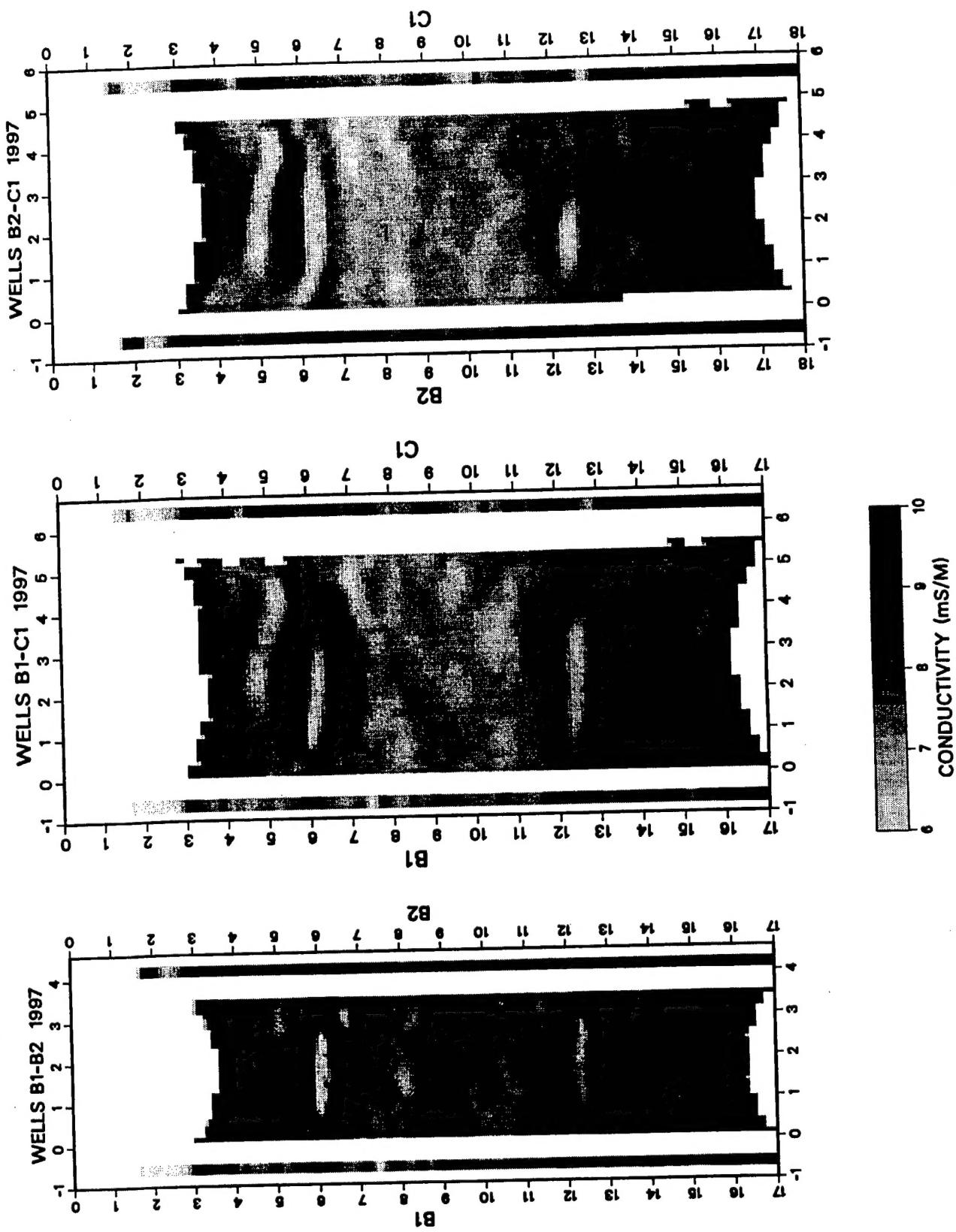
Figure 4. Conductivity tomograms as estimated from the attenuation values using Equation (4). Adjusted conductiity logs are plotted in grey-scale format on either side of the radar tomograms.

637

Figure 6. Seismic velocity tomogram for wells B1-B2.
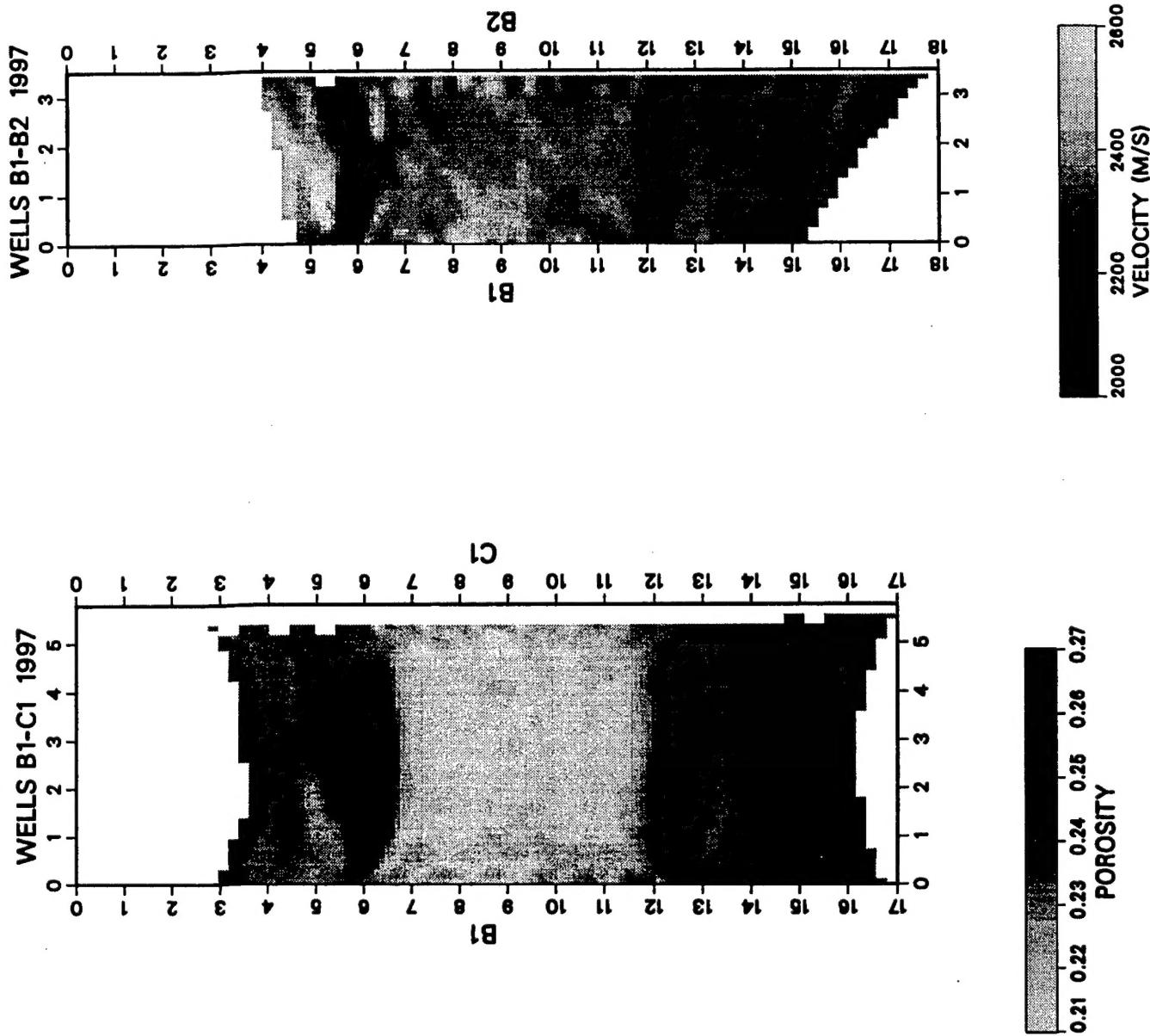
Figure 5. Porosity tomogram using 100 MHz radar antennas.

638